Development of oxide dispersion strengthened W alloys produced by hot isostatic pressing

J. Martínez, B. Savoini, M.A. Monge, A. Muñoz*, R. Pareja

Departamento de Física, Universidad Carlos III de Madrid, 28911 Leganés, Spain

Keywords:
Ultrafine-grained W alloys
Oxide dispersion strengthening
W–Ti alloys
W–V alloys
HIP sintered W alloys

A B S T R A C T

A powder metallurgy technique has been developed to produce oxide strengthened W–Ti and W–V alloys using elemental powders and nanosized powders of La_2O_3 or Y_2O_3 as starting materials. The alloys consolidated by hot isostatic pressing resulted in high-density materials having an ultrafine-grained structure and microhardness values in the range 7–13 GPa. Atom force microscopy studies show a topographic relief in the Ti and V pools that appear in the consolidated alloys. This relief is attributed to the heterogeneous nucleation of martensite plates. The preliminary transmission electron microscopy studies have revealed that a dispersion of nanoparticles can be induced in these alloys produced via the present technique.

1. Introduction

W and its alloys are very promising materials for making plasma facing components in the future fusion power reactors. In particular, these materials are being considered candidate materials for high heat flux components with structural functions in the divertor [1,2]. The properties that make W a suitable material for using as a plasma facing material are its high melting point, good thermal conductivity, high thermal stress resistance, low tritium retention and high temperature strength along with a low sputtering rate.

The lower and upper bounds of the operating temperature range of W, as a structural material, are respectively given by its ductile–brittle transition temperature (DBTT) and its recrystallization temperature (RCT). These temperatures are strongly dependent on the alloying elements, impurities and microstructural characteristics induced by the processing route [3]. Furthermore, the DBTT also depends on the testing method and strain rate. Thus, the reported DBTT and RCT for W exhibit an ample range of values [3–5]. On the other hand, polycrystalline W is brittle at room temperature, what makes the fabrication of W components difficult. Hence, attempts for improving its mechanical behavior have been carried out via addition of alloying elements or stable oxides. For instance, the addition of Re to W lowers the DBTT and enhances its ductility and mechanical characteristics at high temperatures. However, W–Re alloys have been excluded for fusion applications because they suffer severe embrittlement induced by neutron irradiation due to the Re transmutation [6–8]. The dispersion of oxide particles increases the RCT and the strength at high temperature via grain refinement. In case the alloys are produced by mechanical alloying, it is possible to improve the ductility [3].

The current He-cooled divertor designs are considering a thermal armor of sintered W tiles joined to thimbles of oxide dispersion strengthened (ODS) W alloy. These ODS alloys have to be properly joined to sintered W tiles, besides having a low DBTT and a high RCT. This requires the development of ODS W alloys containing an element that enhances the joining using a metal interlayer. In fact, joining between pure W and W–1% La_2O_3 (WL10) is successfully accomplished by a Ti interlayer [9]. The goal of the present work has been the development of different ODS W–V and W–Ti alloys containing Y_2O_3 or La_2O_3.

2. Experimental procedure

Alloys with compositions: W–*x*% Ti–1% La_2O_3, W–4% V–1% La_2O_3 and W–*x*% V–0.5% Y_2O_3 (wt%), $x = 2$ or 4, were produced by a powder metallurgy method using pure W, Ti and V as starting powders. Hereafter the alloys will be referred to as W–*x*TiLa, W–*x*VLa and W–*x*VY. The purity and particle sizes of these powders were 99.9% and <5 μm for W, 99.9% and <110 μm for Ti, and 99.5% and <41 μm for V. In the case of the alloy W–4VLa, the used W powder had an average particle size of 14 μm. To produce oxide dispersion in the alloys, 99.5% pure nanosized powders of either La_2O_3 or Y_2O_3 with particle sizes between ~10 and 50 nm were added. The powder with the target composition was processed and consolidated through a route consisting in four steps: (1) blending of the starting powders in a Turbular T2F mixer for 4 h; (2) mechanical alloying of the powder blends for 20 h at 400 rpm in a high-energy planetary ball mill; (3) encapsulation, and degassing for 24 h at 673 K;

* Corresponding author.
E-mail address: angel.munoz@uc3m.es (A. Muñoz).

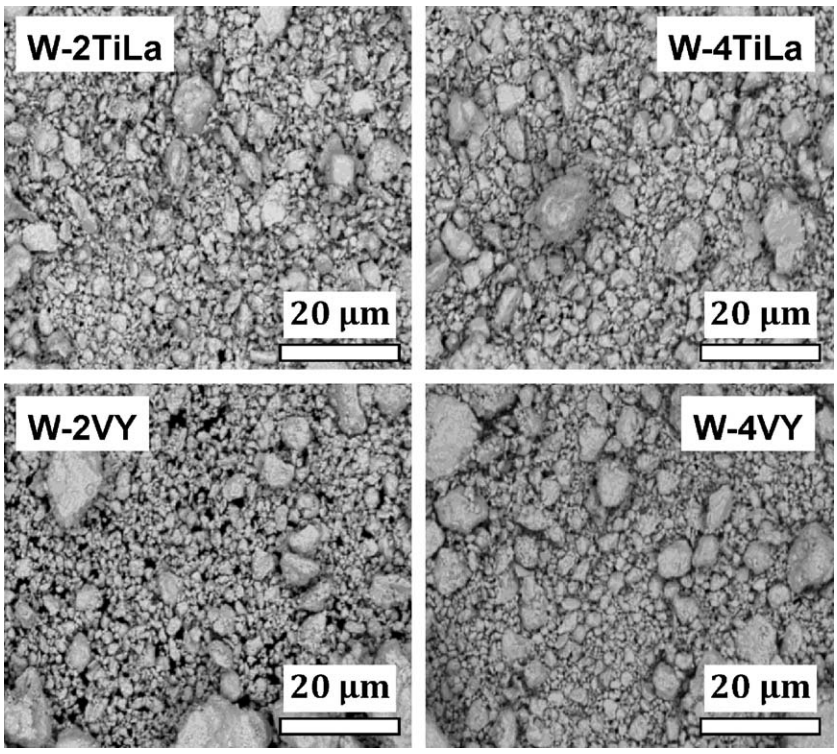

Fig. 1. BSE images showing the prealloyed powders after milling for 20 h.

and (4) sintering by hot isostatic pressing (HIP) for 2 h at 1573 K and 195 MPa.

The mechanical alloying was carried out under a high purity Ar atmosphere in a pot lined with WC, using WC balls of 10 mm in diameter as grinding media at a ball-to-powder ratio of 4:3. The powders were encapsulated in 304 steel cans, which were vacuum sealed after degassing. The handling of the powders, and the process of loading and unloading the pot, was carried out inside a glove box under a high purity Ar atmosphere.

The particle size distribution of the powders was measured by laser light scattering, and the C and O contents in the alloys determined in LECO TC500 and CS-200 elemental analyzers. The C contents in the consolidated materials were about 680 ppm for the W–Ti alloys, and between 180 and 250 ppm for the W–V alloys. The O contents ranged between 0.50 and 0.64 wt% in the W–Ti alloys, and between 0.40 and 0.56 wt% in the W–V alloys. Precise density measurements of the consolidated samples were carried out in a He ultrapycnometer. Vickers microhardness measurements were performed applying a load of 2.94 N for 20 s.

The microstructural characteristics of these alloys have been investigated by X-ray diffraction (XRD), scanning and transmission electron microscopy (SEM and TEM) and atomic force microscopy (AFM). The thin samples for TEM were prepared using a focused ion beam (FIB). XRD patterns were analysed by the Rietveld method using the Fullprof software [10]. The average crystallite size of the milled powders was determined from the diffraction peak widths taking into account the resolution function of the diffractometer.

3. Results and discussion

The particle morphology and size distribution of the blended and milled powders are shown in Fig. 1 and Table 1, respectively. The present milling conditions turned the initial trimodal size distribution of the blended powders into a single mode one, as Fig. 2 reveals for W–4TiLa. The asymmetrical initial shape of the size

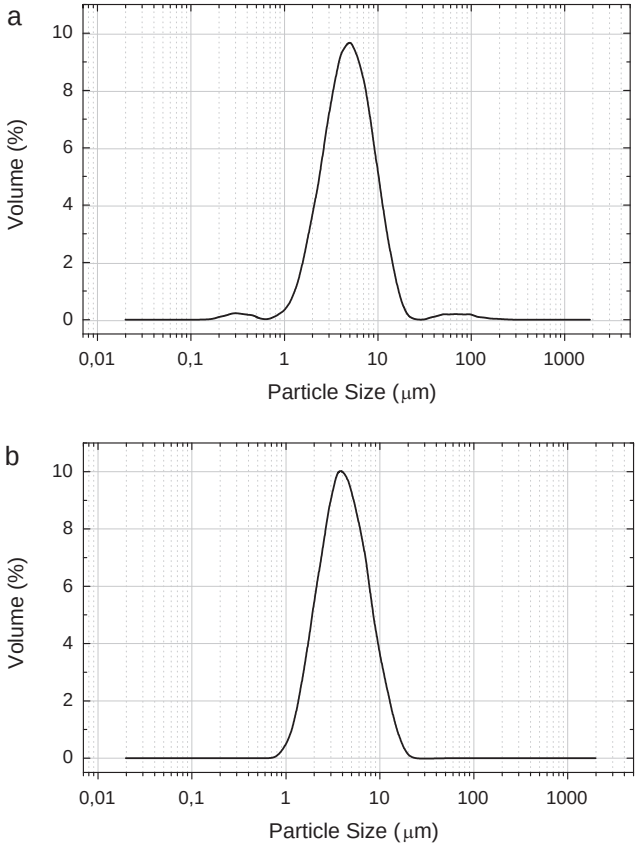

Fig. 2. Particle size distribution for (a) blended and (b) milled W–4TiLa.

Table 1
Particle size distribution for the prealloyed powders after milling for 20 h.

Alloy	Sizes (μm) for fraction of powder		
	10%	50%	90%
W–2TiLa	<2.01	<4.35	<10.18
W–4TiLa	<1.97	<4.15	<8.96
W–4VLa[a]	<3.52	<12.4	<33.4
W–2VY	<1.08	<2.92	<7.38
W–4VY	<1.51	<4.04	<10.30

[a] The starting W powder had an average particle size of 14 μm.

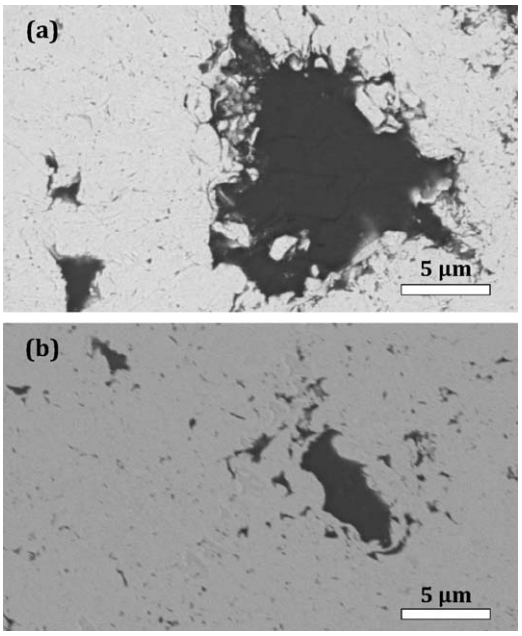

Fig. 3. BSE image showing pools of (a) Ti and (b) V in HIP consolidated W–TiLa and W–4VY, respectively.

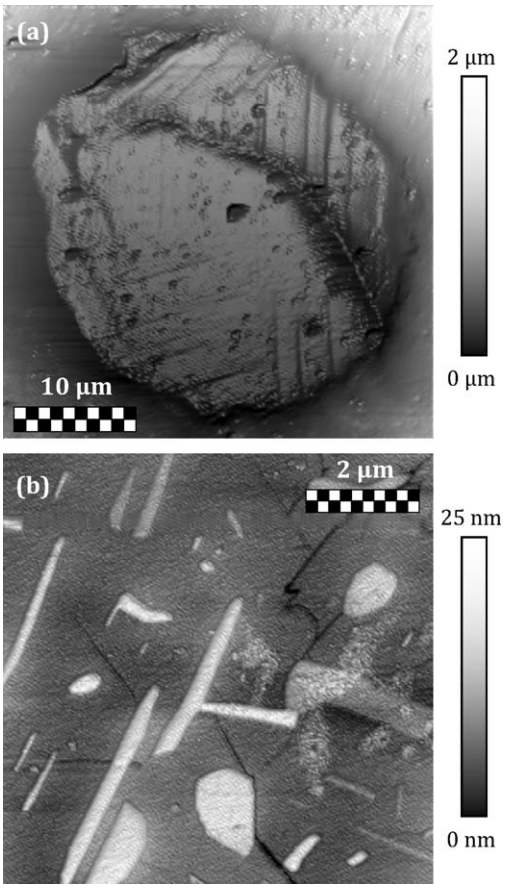

Fig. 4. AFM images showing the surface relief in (a) a Ti and (b) a V pool developed in the alloys W–4TiLa and W–4VLa, respectively.

distribution of the blended powders is retained, and the particle refinement is relatively small.

The analyses of the milled powders by energy dispersion spectroscopy (EDS) and electron backscattering (EBS) images revealed a homogeneous composition for the alloys. Diffraction peaks due to the Ti or V were not detected in the milled powders. It should be noticed that the presence of the Ti phase, even in the case of blended W–4TiLa, cannot be detected because of the strong X-ray absorption by the W atoms.

The average crystallite sizes along with the measured, calculated and relative densities, are given in Table 2. The theoretical densities are calculated applying the mixture rule. The relative densities indicate that the densification degree is acceptable. This appears to increase with the content of Ti or V. The HIP treatment produced the segregation of Ti or V giving rise to the formation of large pools of these elements in the corresponding consolidated material, as shown in Fig. 3. These pools, which sizes as large as ~40 μm, usually exhibited some topographic relief as the AFM images in Fig. 4 reveal for W–4TiLa and W–4VLa. This relief, which were observed in the Ti pools as well as in the V pools, appears to be of martensitic nature. In the case of W–4TiLa, it should be noted that the content of W and other β-stabilizing impurities in the Ti pools could be high enough to favor a $\beta \rightarrow \alpha'$ martensitic transformation [11].

The relief observed in the V pools, originated by the formation of plates, was significantly stronger than the one observed in the Ti pools. The EDS analyses of these plates did not reveal any difference in the chemical composition respect to that found in the corresponding pool. Furthermore, these plates appeared to deflect the propagation of the microcracks, and even impede it, as Fig. 4b reveals. Microcracks were profusely observed in the large V pools that exhibited relief. This suggests the occurrence of large strains in the V pools, likely induced by the thermal stress generated on cooling during the HIP processing of the alloy. Large strains might induce the formation of martensite plates, heterogeneously distributed, as reported for V–1.6% Y neutron irradiated [12].

TEM images revealed a grain structure with sizes typically smaller than ~0.5 μm, as shown in Fig. 5 for W–4VLa. The preliminary TEM studies performed on W–4VLa have also revealed

Table 2
Density, microhardness and average crystallist size for the consolidated alloy.

Alloy	Calculated (g/cm^3)	Measured (g/cm^3)	Relative %	HV (GPa)	Size (nm)
W–2TiLa	17.699	17.235	97.36	13.3 ± 0.5	52
W–4TiLa	16.695	16.707	100.07	8.6 ± 0.5	29
W–4VLa[a]	17.368	16.940	97.54	7.4 ± 0.5	130[a]
W–2VY	18.209	17.830	97.92	12.4 ± 0.3	16
W–4VY	17.498	17.267	98.80	13.1 ± 0.6	15

[a] The starting W powder had an average particle size of 14 μm.

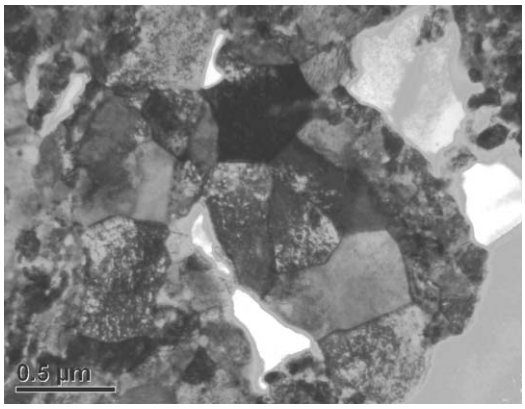

Fig. 5. TEM image showing the ultrafine grain structure obtained in the W–4VLa alloy.

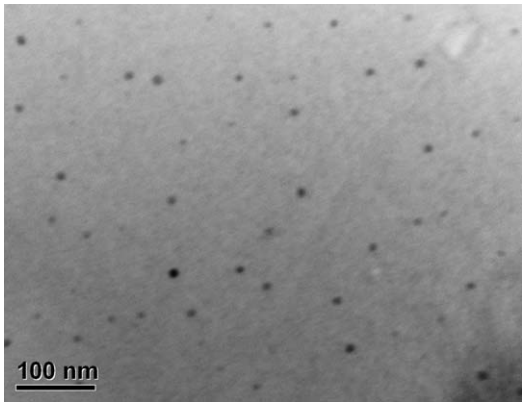

Fig. 6. TEM image showing the dispersion of nanoparticles developed in the W–4VLa alloy.

the formation of a dispersion of La-rich nanoparticles, as Fig. 6 reveals. Further studies to confirm the presence of a similar dispersion in the other alloys, and determine the specific composition of the nanoparticles, are presently underway.

The mechanical characterization of these alloys is now in progress. The preliminary three point bending tests have shown that the bending strength and fracture toughness are significantly enhanced in comparison with unalloyed W processed by the same route [13].

4. Conclusions

1. Ultrafine-grained and high-density W–Ti and W–V alloys containing La_2O_3 or Y_2O_3 have been obtained by mechanical alloying and subsequent consolidation by HIP.
2. Under the present processing conditions, a dispersion of nanoparticles can be developed in these alloys.
3. The alloys consolidated by HIP showed large dispersed pools of Ti or V with microcracks and relief in their surfaces. This relief might be due to a heterogeneous nucleation of stress-induced martensite plates in these pools. These plates appear to have the capability of deflecting or blocking the propagation of the microcracks.

Acknowledgments

The TEM and SEM studies were carried out at the Materials Department of Loughborough. The authors express their gratitude to Dr. di Martino for his assistance in these studies. This investigation was supported by the Comunidad de Madrid (program ESTRUMAT-CM S0505/MAT/0077) and Spanish Ministry of Science and Innovation (contract ENE2008-06403-C06-04), with additional contributions from EURATOM/CIEMAT association through contract EFDA WP08-09-MAT-WWALLOY.

References

[1] J.W. Davis, V.R. Barabash, A. Makhankov, L. Plöchl, K.T. Slattery, J. Nucl. Mater. 258–263 (1998) 308–312.
[2] H. Bolt, V. Barabash, W. Krauss, J. Linke, R. Neu, S. Suzuki, N. Yoshida, ASDEX Upgrade Team, J. Nucl. Mater. 329–333 (2004) 66–73.
[3] I. Smid, M. Akiba, G. Vieider, L. Plöchl, J. Nucl. Mater. 258–263 (1998) 160–172.
[4] M. Rieth, B. Dafferner, J. Nucl. Mater. 342 (2005) 20.
[5] M. Faleschini, H. Kreuzer, D. Kiener, R. Pippan, J. Nucl. Mater. 367–370 (2007) 800.
[6] F.W. Wiffen, Proceedings of Symposium on Refractory Alloy Technology for Space Nuclear Power Applications, Oak Ridge, TN, USA, 1983, p. 252.
[7] R.K. Williams, F.W. Wiffen, J. Bentley, J.O. Siegler, Metall. Trans. 14A (1983) 655–666.
[8] M. Schuster, I. Smid, G. Leichtfried, Physica B 234–236 (1997) 1224–1226.
[9] P. Norajitra, A. Gervash, R. Giniyatulin, T. Ihli, W. Krauss, R. Kruessmann, V. Kumetsov, A. Makhankov, I. Mazul, I. Ovchinnikov, Fus. Eng. Des. 81 (2006) 341–346.
[10] J. Rodriguez-Carvajal, Physica B 192 (1993) 55.
[11] S. Banerjee, P. Mukhopadhyay, Phase Transformation: Examples from Titanium and Zirconium Alloys, Pergamon Series Materials 12 (2007) 281.
[12] H. Kurishita, S. Kobayashi, K. Nakai, Kuwabara, M. Hasegawa, J. Nucl. Mater. 358 (2006) 217–226.
[13] A. Muñoz, J.Y. Pastor, R. Pareja, M.A. Monge, B. Savoi, T. Leguey, et al., 1st Monitoring Meeting of MAT-W&W Alloys Project, in: EFDA, Garching, Germany, 2010.